



Breaking Anchored Droplets in a Microfluidic Hele-Shaw Cell

Gabriel Amselem,¹ P. T. Brun,^{2,*} François Gallaire,² and Charles N. Baroud^{1,†}

¹*LadHyX and Department of Mechanics, Ecole Polytechnique, CNRS, 91128 Palaiseau Cedex, France*

²*LFMI, EPFL, Lausanne, Switzerland*

(Received 1 December 2014; revised manuscript received 18 March 2015; published 12 May 2015)

We study microfluidic self-digitization in Hele-Shaw cells using pancake droplets anchored to surface-tension traps. We show that above a critical flow rate, large anchored droplets break up to form two daughter droplets, one of which remains in the anchor. Below the critical flow velocity for breakup, the shape of the anchored drop is given by an elastica equation that depends on the capillary number of the outer fluid. As the velocity crosses the critical value, the equation stops admitting a solution that satisfies the boundary conditions; the drop breaks up in spite of the neck still having finite width. A similar breaking event also takes place between the holes of an array of anchors, which we use to produce a 2D array of stationary drops *in situ*.

DOI: 10.1103/PhysRevApplied.3.054006

I. INTRODUCTION

One of the underlying drivers in microfluidics is to miniaturize the standard multiwell plate and transform it into an integrated programmable device, while replacing the hundreds of wells typical today with thousands or more nanoliter-scale compartments. Early success has been achieved by using deformable chambers that could be opened or closed using an external pressure source [1]. In parallel, droplet-based microfluidics continues to attract ever-increasing interest since it provides an elegant way to encapsulate an initial sample into a large number of independent microcompartments. However, the traditional droplet production and manipulation methods all rely on the drops flowing in a row in a linear microfluidic channel. Studying the contents of these drops [2,3] is, therefore, more akin to flow cytometry than to multiwell plates.

Recently, several groups have shown how to array droplets in microfabricated traps, particularly in a wide two-dimensional (2D) region [4,5]. These devices typically allow a droplet density of several hundred per cm², far beyond what is currently possible outside microfluidics. Nevertheless, these devices must still be coupled to a traditional drop production device before they are brought to the observation chamber. While the underlying physical mechanisms for these drop production devices is now well understood [6,7], they are poorly adapted in practice to making a limited number of stationary drops. For this reason, quasi-two-dimensional devices have been designed to break an initially large drop into stationary subdroplets that are held in pockets on the side of a sinuous channel

[8–10], while truly 2D devices allow much higher density of trapped droplets [11].

Here we describe the ability to break droplets *in situ* in a wide chamber, by pushing them over a truly two-dimensional array of microfabricated traps [12]. We elucidate the physical mechanisms first on a single droplet and show that it is well described by a set of universal curves given by the elastica equation. The drop then breaks through a singularity in the curves beyond a critical deformation, leading to a well-characterized and robust size. In addition to its applications for droplet arrays, this route to breaking a liquid interface provides fundamental insight into the evolution of drops and bubbles in all confined geometries, where the traditional Rayleigh-Plateau instability is not active.

II. EXPERIMENTAL SETUP

The experimental setup consists of a wide chamber (width $w = 2.5$ mm) in which the drops can be anchored in a central trap, as shown in Figs. 1(a) and 1(b). The chamber height h and the anchor diameter d are in the range 35–50 μm and 75–200 μm , respectively. The height of the anchor e is chosen to be of the order of the height of the channel. All devices are made out of polydimethylsiloxane (PDMS, Dow Corning). The droplets studied here are produced by a flow-focusing junction upstream of the chamber [Fig. 1(b)], designed such that the drops are forced to adopt a pancake shape of radius $R \gg h$ in the chamber. Droplets of fluorinated oil are produced in a glycerol-water mixture with 2% sodium dodecyl sulfate (SDS) as a surfactant. The oil viscosities μ_{oil} range between 1.2 and 24 cP, whereas the outer phase viscosity μ varies between 0.89 and 3.3 cP by varying the water-to-glycerol ratio. The interfacial tension between the drop and the outer liquid has a typical value $\gamma \sim 17$ mN/m.

*Present address: Department of Mathematics, Massachusetts Institute of Technology, Cambridge, MA 02139, USA.

†baroud@ladhyx.polytechnique.fr

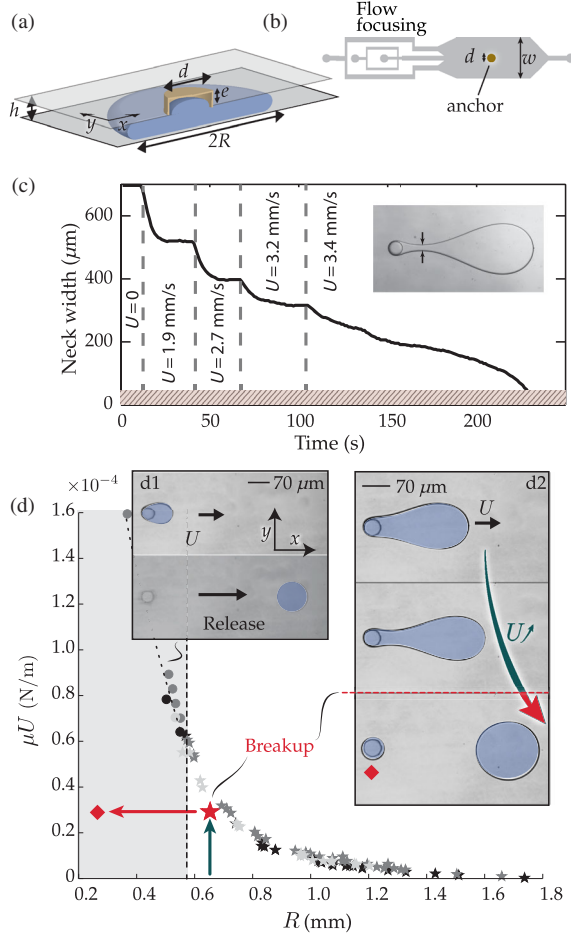


FIG. 1. (a) Schematic of an anchor of diameter d and height e , trapping a drop of radius R (no external flow); the chamber height is h . (b) Sketch of the microfluidic device: droplets are produced with a flow focuser and trapped on an anchor centered in the observation chamber, $w = 2.5$ mm. (c) Typical evolution of the droplet neck width (see inset) as the outer flow velocity U is increased. When the critical velocity is passed, the neck never reaches a stationary state; instead, it decreases until it matches the channel height ($h = 49$ μm), where it becomes unstable by Rayleigh-Plateau instability. (d) For a given microchannel, a trapped droplet either escapes from its anchor at a critical value of the capillary number (grayed area, $R \lesssim 600$ μm) or breaks on the anchor ($R \gtrsim 600$ μm), leaving a smaller droplet behind. Experimental points for droplets of FC-40 in glycerol-water mixtures of different viscosities: $\mu = 0.93$ cP (dark gray), $\mu = 1.6$ cP (medium gray), and $\mu = 3.3$ cP (black). SDS is used as a surfactant at a concentration of 2% in all cases.

During a typical experiment, a droplet is anchored on a surface energy trap, and the outer velocity is increased step by step. A typical measurement of the drop evolution is shown in Fig. 1(c), where the smallest width of the drop neck is reported. We observe that the neck reaches a stationary value when the outer fluid is flowing below the critical velocity. At the critical velocity, the neck begins to decrease from a finite value, slowly at first, but then this decrease is accelerated until the neck width becomes equal

to the channel height. Because of this loss of confinement locally, the Rayleigh-Plateau instability becomes active and the neck breaks, as observed previously for different droplet production situations [6,7,13].

For a given setup and droplet volume, we find that there exists a critical capillary number $\text{Ca}^* = \mu U^*/\gamma$ above which the droplet either escapes from the anchor [12] [Fig. 1(d1)], or breaks on the anchor [Fig. 1(d2)]. In this second regime, the drop leaves behind a daughter droplet small enough to remain anchored at the breakup velocity U^* : the daughter droplet lies in the trapped region of the phase diagram, as indicated by the diamond in Fig. 1(d). In the rest of this paper, we focus on the breakup regime exclusively.

III. RESULTS AND DISCUSSION

A. Droplet shape: Theory and experiments

The droplet stationary shapes are imposed by the pressure difference between the two sides of the interface. The flat microfluidic chamber can be modeled as a Hele-Shaw cell, so we adopt a two-dimensional depth-averaged formalism to describe the system. Then, the pressure drop in the flow direction x is related to the average flow velocity U according to

$$p_o(x) = -24 \frac{\mu U}{h^2} x + \text{const}, \quad (1)$$

where $p_o(x)$ is the pressure in the outer aqueous phase. The pressure p_i inside the oil drop is constant [12,14] and is related to the outside pressure $p_o(x)$ by the Laplace relation:

$$p_i - p_o(x) = \gamma \left(\kappa_{\perp} + \frac{\pi}{4} \kappa_{\parallel} \right), \quad (2)$$

where κ_{\perp} and κ_{\parallel} are the curvatures in the perpendicular and the parallel planes, respectively [15]. Away from the anchor, the curvature in the perpendicular plane is assumed constant $\kappa_{\perp} = 2/h$.

The droplet 2D shape $\mathbf{r}(s)$, where s denotes the interface arclength, is described in Fig. 2(b). The tangent to the droplet interface is obtained by differentiating the position with respect to the arclength $\mathbf{r}'(s) = (\cos \theta(s), \sin \theta(s))$, and the in-plane curvature is given by $\kappa_{\parallel} = \theta'(s)$. Differentiating Eq. (2) with respect to s and using Eq. (1) in the particular case where $x = \mathbf{r}(s) \cdot \mathbf{e}_x$ yields an elastica equation:

$$\theta''(\bar{s}) - \frac{R^2}{\ell^2} \cos \theta(\bar{s}) = 0, \quad (3a)$$

where $\ell = h\sqrt{\pi/96}\text{Ca}^{-1/2}$ denotes the “viscocapillary length” of the problem, and the radius R of the undeformed droplet is used to nondimensionalize the problem (nondimensional variables, such as \bar{s} , are denoted with a bar). Equation (3a) is a 2D pendant drop equation [12,16].

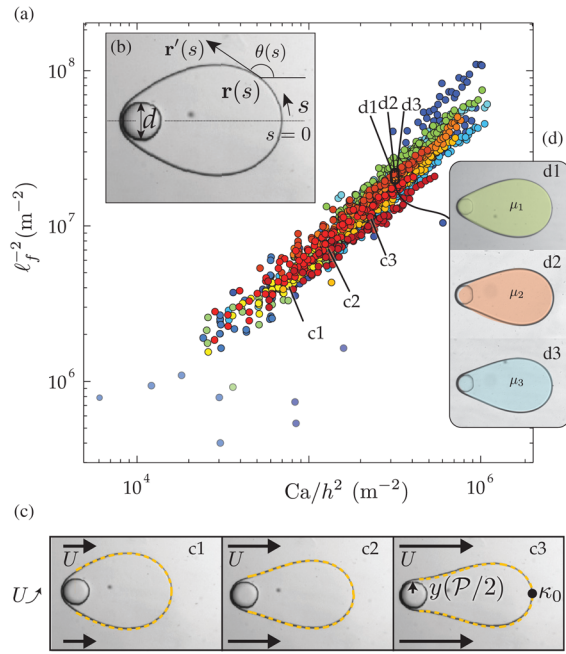


FIG. 2. (a) Evolution of the fitting parameter ℓ_f with the value of Ca/h^2 , for different channel heights, trap diameters, and droplet fluid viscosities. The cloud of data points confirms that $\ell^{-2} \sim Ca/h^2$. (b) Photograph of an anchored droplet under flow and system of coordinates in which the interface $\mathbf{r}(s)$ is derived. s is the arclength along the interface, and $\mathbf{r}'(s)$ is its tangent. (c) From left to right: Droplet shape for increasing outer fluid velocities. Orange dotted lines are the best-fitting elastica shape. (d) Three droplets of different viscosities ($\mu_1 = 1.2$, $\mu_2 = 4.1$, $\mu_3 = 24$ cP) but similar volumes, for the same value of $\mu U/\gamma h^2$: the droplet shape is independent of the droplet viscosity.

Note that the droplet shape does not depend on its viscosity: the only viscosity entering the problem (through ℓ) is the external fluid viscosity. To qualitatively check this prediction, we show in Fig. 2(d) the shapes of three different droplets of different viscosities (between 0.77 and 24 cP) but similar volumes and at the same value of Ca . The drops, indeed, have similar shapes that cannot be distinguished from each other.

Secondary variables are now defined to ease the integration of the problem. The cumulative dimensionless area swept by the droplet interface $\bar{\alpha}(\bar{s})$ is defined as the solution of

$$\bar{\alpha}'(\bar{s}) = \bar{y}(\bar{s})\bar{x}'(\bar{s}). \quad (3b)$$

The drop shape is obtained by integrating Eqs. (3a) and (3b) with a shooting method. For given values of \bar{d} and $\bar{\ell}$, we use the curvature $\bar{\kappa}_0 = \bar{\kappa}_{||}(\bar{s} = 0)$ as the sole shooting parameter and search for the values of $\bar{\kappa}_0$ that satisfy the geometric condition $\bar{y} = \bar{d}$ at $\bar{\alpha} = \pi/2$. The droplet shape $\mathbf{r}(s)$ is then fully defined by the triplet $\{\bar{d}, \bar{\ell}, \bar{\kappa}_0\}$.

The calculations of $\bar{\kappa}_0$ are first performed for different values of $\bar{\ell}$, while keeping \bar{d} constant, and the whole process is repeated for different values of \bar{d} . This leads to a catalog of shapes that can be used to fit the experimental droplet shapes. For each experimental condition, the best-fitting shape is found, and its associated triplet is called $\{\bar{d}_f, \bar{\ell}_f, \bar{\kappa}_{0f}\}$. Since all numerical shapes are obtained using dimensionless variables, it is also necessary to redimensionalize them, and we call R_f the radius of the best-fitting shape for each fit. There is a very good agreement between numerical and experimental shapes, as shown in Fig. 2(c). We also find excellent agreement between R_f and R , with a difference of at most 5% between both values, the best fits being obtained for low values of ℓ .

A quantitative comparison between theory and experiments is obtained by comparing the evolution of the fitting parameter $\ell_f^{-2} = R_f^2/\ell_f^2$ with the experimental value of Ca/h^2 . The resulting values are plotted in Fig. 2(a), which displays the data for different channel geometries, droplet and outer fluid viscosities, and trap diameters. The data verify the scaling predicted by theory $\ell^{-2} \sim Ca/h^2$, with a prefactor (approximately 60) that differs from the prediction ($96/\pi \approx 31$), most likely because of dynamic surfactant effects [12]. Taken together, the above results show that the droplet shape is well described by the elastica for forcing values below the breaking threshold.

B. Droplet breakup: Theory and experiments

We now turn to the breaking. The solutions to the elastica equation can be plotted as a family of curves in the $(\bar{\kappa}_0, 1/\bar{\ell}^2)$ plane, for different values of \bar{d} ; see Fig. 3(a). The curves all display a monotonic increase of $\bar{\kappa}_0$ with $1/\bar{\ell}^2$ until a maximum value of $1/\bar{\ell}^2$ where they reach a turning point, and after which no values of $\bar{\kappa}_0$ are found. The folding of the branch of solutions is associated to an exchange of stability at the marginally stable turning point. This implies that no stationary solutions to the elastica equation can be found beyond this point, and the equilibrium can be reached only through a dynamic process which is not accounted for by the static model. We call $\bar{\ell}^*$ the value of $\bar{\ell}$ at the turning point of the curve and, therefore, expect that the droplet will break at $\bar{\ell} = \bar{\ell}^*$ even though the droplet neck still has a finite width, as shown in the inset of Fig. 3(a).

Experimentally, increasing quasistatically the flow rate around a droplet pinned on an anchor amounts to walking along a curve with increasing $1/\bar{\ell}^2$. This leads to an increase in $\bar{\kappa}_0$ until the value of $\bar{\ell} = \bar{\ell}^*$ is reached, corresponding to a critical velocity U^* beyond which there are no stationary solutions. For each experiment, we compare the fitted value of $\bar{\ell}_f^*$ with the predicted value $\bar{\ell}^*$ in Fig. 3(b). The agreement between the two is remarkable, confirming the interpretation of the breaking:

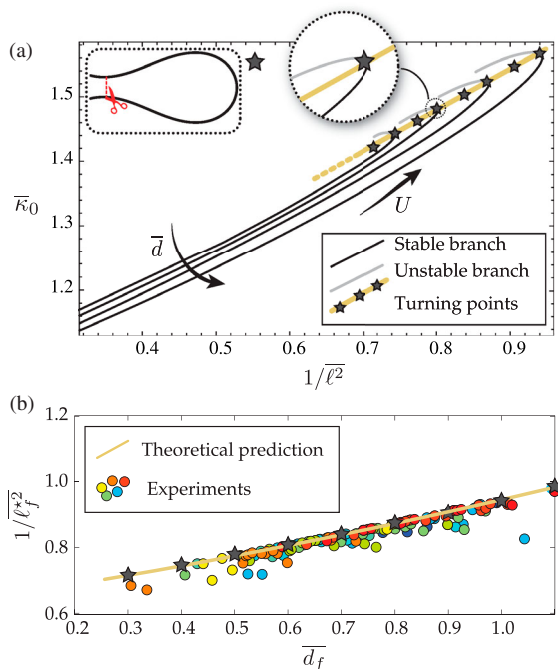


FIG. 3. (a) Branches of solutions of the elastica shown in the plane $(1/\ell^2, \bar{\kappa}_0)$, each corresponding to a given value of \bar{d} . The stable part (unstable) is denoted with a black line (gray line). For a given \bar{d} , the critical value $1/\ell^{*2}$ at which the drop breaks is indicated by a star corresponding to the turning point of the branch of solutions. Yellow line shows the interpolation of a discrete number of turning points. Inset: Shape of the anchored drop at the critical value of $1/\ell^{*2}$. (b) Comparison between experimental values of $1/\ell_f^{*2}$ at which the drops break with the theoretical prediction from part (a).

above the velocity U^* , no equilibrium droplet shape can be found that satisfies the elastica equation with the imposed boundary conditions. We find that the larger \bar{d}_f , the larger the value of $1/\ell_f^*$; i.e., in a given experimental setup with a fixed trap diameter d , the critical velocity U^* leading to breakup is smaller for large droplets than it is for small droplets.

In many situations it is important to determine the volume of the trapped fluid in the anchor, for example, if the device is used to observe biological samples. This determination is equivalent to predicting, in our 2D view, the projected area \mathcal{A}_d of the droplet left on the anchor after breakup. We expect the area to depend both on the diameter of the trap d and on the droplet radius R . The dependence of \mathcal{A}_d on d is dictated by the boundary condition that the trap imposes on the droplet shape. The dependence on R comes from the geometry of the breakup: we experimentally and numerically observe that, for a given d , the pinch-off distance from the anchor increases with R , occurring farther downstream of the trap for larger drops. Rescaling all lengths by R , we show the evolution of the dimensionless area \mathcal{A}_d/R^2 as a function of $\bar{d} = d/R$ for both experimental

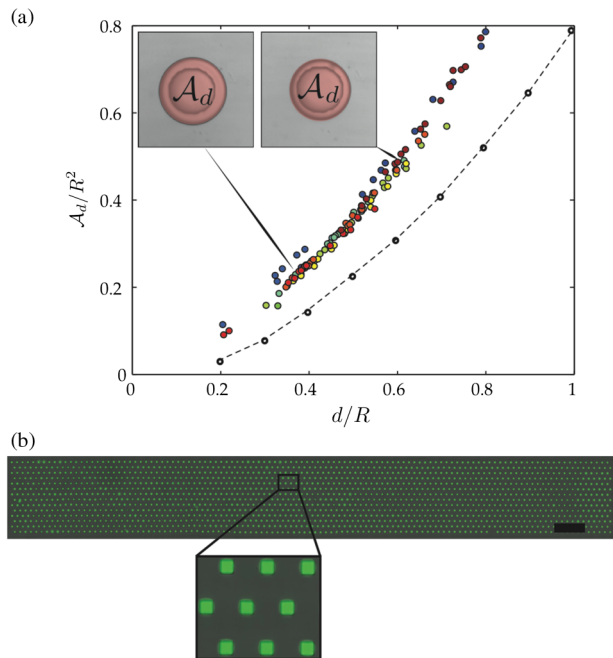


FIG. 4. (a) Remaining area (dimensionless) as a function of $\bar{d} = d/R$. Dots: experiments. Line: theoretical prediction. Insets: Two droplets of different sizes left on the same anchor ($d = 150 \mu\text{m}$) by two different drops. (b) An array made up of 1568 individual drops produced through self-digitization. The aqueous solution contains fluorescein to aid in the visualization. We use square anchors with side $d = 130 \mu\text{m}$ in a channel of height $h = 35 \mu\text{m}$. Scale bar: 2 mm.

results and theoretical simulations in Fig. 4(a). Note that a perfect agreement cannot be expected between the theoretical and experimental results since the model is 2D, whereas 3D effects are present close to the anchor. Still, the trends of the two curves are identical.

IV. CONCLUSION

We now examine the practical implications of the demonstrated method. A droplet breaks on an anchor as long as the outer flow velocity satisfies $U > U^*$. In this sense, one does not need a precise flow control to produce a droplet: pushing the outer flow using a hand-held syringe is sufficient to break droplets. Also, the only relevant viscosity coming into play is the viscosity μ of the outer fluid: since U^* does not depend on the inner fluid viscosity, the singularity occurs at the same time for droplets of a given volume so that there is no difference between breaking droplets of a viscous fluid such as Fluorinert FC-70 (3M) ($\mu = 24 \text{ cP}$) or breaking droplets of Novec fluid HFE-7500 239 (3M) ($\mu = 1.2 \text{ cP}$). The volume left on the trap is dependent on the geometries of the trap and that of the drop: the sole important dimensionless parameter is \bar{d} . Therefore, whatever the fluids used, their surface tensions, or viscosities, two drops of the same volume will break on

an anchor of diameter d into droplets of the same size \mathcal{A}_d that depends solely on d and R .

The breakup of a single droplet can be generalized to an array of traps of any dimension, as shown in Fig. 4(b), which shows an array of 112×14 drops. In this experiment, an aqueous “puddle” initially fills the chamber and is then pushed by a flow of a wetting oil. The drops, which are produced at 10 Hz, detach as the front passes the anchors. Again, the interface connecting two anchors is described by an elastica equation, albeit with different boundary conditions than the single anchor, and breaks when the enclosed volume is reduced below a critical value. Such devices are directly applicable to bioassays and preview droplet-based microfluidic multiwell plates.

ACKNOWLEDGMENTS

The authors thank Caroline Frot for help with the microfabrication and David Gonzalez-Rodriguez for helpful discussions. The research leading to these results received funding from the European Research Council under the European Unions Seventh Framework Programme (FP7/2007- 2013) and ERC Grant No. 278248 MULTICELL for Ecole Polytechnique, and ERC Grant No. 280117 “SIMCOMICS” for EPFL.

-
- [1] T. Thorsen, S. Maerkl, and S. Quake, Microfluidic large-scale integration, *Science* **298**, 580 (2002).
- [2] H. Song and R. Ismagilov, Millisecond kinetics on a microfluidic chip using nanoliters of reagents, *J. Am. Chem. Soc.* **125**, 14613 (2003).
- [3] O. J. Miller, A. E. Harrak, T. Mangeat, J. -C. Baret, L. Frenz, B. E. Debs, E. Mayot, M. L. Samuels, E. K. Rooney, P. Dieu, M. Galvan, D. R. Link, and A. D. Griffiths, High-resolution dose-response screening using droplet-based microfluidics, *Proc. Natl. Acad. Sci. U.S.A.* **109**, 378 (2012).
- [4] A. Huebner, D. Bratton, G. Whyte, M. Yang, A. deMello, C. Abell, and F. Hollfelder, Static microdroplet arrays: A microfluidic device for droplet trapping, incubation and release for enzymatic and cell-based assays, *Lab Chip* **9**, 692 (2009).
- [5] P. Abbyad, R. Dangla, A. Alexandrou, and C. N. Baroud, Rails and anchors: Guiding and trapping droplet micro-reactors in two dimensions, *Lab Chip* **11**, 813 (2011).
- [6] P. Garstecki, H. A. Stone, and G. M. Whitesides, Mechanism for Flow-Rate Controlled Breakup in Confined Geometries: A Route to Monodisperse Emulsions, *Phys. Rev. Lett.* **94**, 164501 (2005).
- [7] V. van Steijn, C. R. Kleijn, and M. T. Kreutzer, Flows around Confined Bubbles and Their Importance in Triggering Pinch-Off, *Phys. Rev. Lett.* **103**, 214501 (2009).
- [8] H. Boukellal, Š. Selimović, Y. Jia, G. Cristobal, and S. Fraden, Simple, robust storage of drops and fluids in a microfluidic device, *Lab Chip* **9**, 331 (2009).
- [9] A. Yamada, F. Barbaud, L. Cinque, L. Wang, Q. Zeng, Y. Chen, and D. Baigl, Oil microsealing: A robust micro-compartmentalization method for on-chip chemical and biological assays, *Small* **6**, 2169 (2010).
- [10] D. E. Cohen, T. Schneider, M. Wang, and D. T. Chiu, Self-digitization of sample volumes, *Anal. Chem.* **82**, 5707 (2010).
- [11] T. Wu, K. Hirata, H. Suzuki, R. Xiang, Z. Tang, and T. Yomo, Shrunken to femtolitre: Tuning high-throughput monodisperse water-in-oil droplet arrays for ultra-small micro-reactors, *Appl. Phys. Lett.* **101**, 074108 (2012).
- [12] R. Dangla, S. Lee, and C. N. Baroud, Trapping Microfluidic Drops in Wells of Surface Energy, *Phys. Rev. Lett.* **107**, 124501 (2011).
- [13] B. Dollet, W. van Hoeve, J. P. Raven, P. Marmottant, and M. Versluis, Role of the Channel Geometry on the Bubble Pinch-Off in Flow-Focusing Devices, *Phys. Rev. Lett.* **100**, 034504 (2008).
- [14] M. Nagel, P.-T. Brun, and F. Gallaire, A numerical study of droplet trapping in microfluidic devices, *Phys. Fluids* **26**, 032002 (2014).
- [15] C. Park and G. Homsy, Two-phase displacement in Hele Shaw cells: Theory, *J. Fluid Mech.* **139**, 291 (1984).
- [16] S. Majumdar and D. Michael, The equilibrium and stability of two dimensional pendent drops, *Proc. R. Soc. A* **351**, 89 (1976).